7-15-2015

A Computational Method to Predict and Study Underwater Noise due to Pile Driving

Scott Schecklman
Portland State University

Nathan Laws
Portland State University

Lisa M. Zurk
Portland State University, zurkl@pdx.edu

Martin Siderius
Portland State University, siderius@pdx.edu

Citation Details

Schecklman, S., Laws, N., Zurk, L. M., & Siderius, M. (2015). A computational method to predict and study underwater noise due to pile driving. The Journal of the Acoustical Society of America, 138(1), 258-266.

A computational method to predict and study underwater noise due to pile driving

Scott Schecklman, Nathan Laws, Lisa M. Zurk,[a] and Martin Siderius
Electrical and Computer Engineering, Portland State University, Portland, Oregon 97201, USA

(Received 15 July 2014; revised 13 April 2015; accepted 28 May 2015; Published online 15 July 2015)

A hybrid modeling approach that uses the parabolic equation (PE) with an empirical source model is presented to study and predict the underwater noise due to pile driving in shallow, inhomogeneous environments over long propagation ranges. The empirical source model uses a phased point source array to simulate the time-dependent pile source. The pile source is coupled with a broadband application of a PE wave propagation model that includes range dependent geoacoustic properties and bathymetry. Simulation results are shown to be in good agreement with several acoustic observations of pile driving in the Columbia River between Portland, OR and Vancouver, WA. The model is further applied to predict sound levels in the Columbia River and study the effects of variable bathymetry and sediment configurations on underwater sound levels.
 [http://dx.doi.org/10.1121/1.4922333]

[BTH] Pages: 258–266

I. INTRODUCTION

Impact pile driving is used in numerous applications of construction involving marine environments, such as bridge construction and wind farm installation, and can result in extremely high underwater sound levels,[1] which may have harmful physical and behavioral effects on wildlife. Physical effects in fish can include swim bladder rupture, torn tissue, bruising, and hearing loss,[2,3] Behavioral effects are less understood, but can include altered migratory patterns and behaviors leading to increased predation.[4] Deleterious effects also extend to mammals, such as seals, and sediment bound life, such as fish eggs.[5,6] In all types of marine wildlife, specific harmful effects are highly species dependent and are currently an area of ongoing research.

The prediction of underwater sound levels is important for the assessment and eventual mitigation of environmental impacts. Regulatory agencies, such as the California Department of Transportation, currently rely on the practical spreading model (PSM).[7] The PSM is a scaled logarithmic model that relies on curve fitting to acoustic measurements and does not predict frequency dependent levels, time domain characteristics, or the effects of range dependent variations. Recently, Reinhall and Dahl presented a Mach wave description of the pile driving source[8] based on finite element analysis and array measurements that were propagated using parabolic equation (PE) techniques. Good agreement was found between the model and observed data, but the maximum range of comparison was only 17 m, where the effects of range dependent bathymetry and sediment variations are small. Broadband PE techniques have been applied to predict pile driving sound levels at long range, using only a simple source in a deep water environment.[9]

Here, a hybrid PE/empirical source modeling approach is presented to study and predict the underwater noise produced by pile driving that is suitable for use over long ranges in shallow water, range dependent environments. The acoustic noise is propagated by a broadband application of the PE wave propagation model that includes range dependent geoacoustic properties and bathymetry. Coupled into the sound propagation model is an empirical pile source model adapted from the work of Reinhall and Dahl.[8] Simulated results are shown to be in good agreement in both time and frequency domain comparisons with acoustic measurements of test pile operations leading up to construction of the proposed Interstate 5 (I-5) span over the Columbia River between Portland, OR and Vancouver, WA. The method is subsequently applied to generate sound level predictions in the Columbia River and study the effects of variable bathymetry and sediment configurations.

II. SOUND PROPAGATION

This section discusses two methods for computing sound energy levels radiated into the water column from a pile after it is stuck by an impact hammer. The PSM is introduced as a conventional modeling technique that fits a range dependent exponential loss curve with a series of *in situ* sound measurements recorded in the water column at various ranges from the pile. The remainder of the paper presents a hybrid PE/empirical source modeling approach that is similar to the one introduced by Reinhall and Dahl.[8] The hybrid PE/empirical source model uses the PE propagation model to compute the Green's function for a series of point sources distributed along the length of the pile, and then convolves each of the Green's functions with an source spectrum that is derived from a single *in situ* acoustic measurement recorded in the water column near the pile source.

A. Practical Spreading Model

Pile driving is often conducted in shallow water environments, where sound propagation is similar to that through

[a]Electronic mail: zurkl@pdx.edu

a Pekeris waveguide[10] formed by the air-water and lossy sediment boundaries. The PSM is an attempt to combine the transmission loss due to geometric spreading and lossy sediments into a simple model. This model evaluates the total sound exposure level (SEL) at range r. SEL is the discrete time integral of the impact waveform in units of dB re: μPa^2 s. The PSM computes the SEL for a single pile strike, SEL_p, by subtracting the scaled logarithm of range from an assumed source level,

$$SEL_p = SC - F \log r. \tag{1}$$

Here SC is the assumed SEL at the source and F is a constant factor that can vary from 5 to 30 to accommodate the variable attenuation of different channels. For regulatory purposes, the cumulative sound exposure level, SEL_c, is often used,

$$SEL_c = SEL_p + 10 \log N, \tag{2}$$

where N is the total number of pile strikes.

The PSM is problematic because it assumes an environment that is homogeneous, axisymmetric and range independent, while variations in these factors can result in significantly different sound levels. Furthermore, the SC and F parameter cannot be easily obtained, and must be determined by fitting acoustic data at several ranges. Figure 1 shows PSM solutions computed for an SC of 206 dB and F parameters of 5, 10, and 15. This illustrates the sensitivity of sound level predictions to variable F parameters, because, based on the F parameter, the range that is required for the level to drop below a threshold varies dramatically. Finally, the model only produces a simple level prediction and yields no information about time, spectral, or depth dependent sound characteristics. Improvement upon this method requires the computation of physics-based sound propagation and range dependent models of sediment and bathymetry.

B. Parabolic Equation model

Pile-driving in underwater environments is often preceded by civil engineering studies that include fathometer measurements and boring logs to quantify the local bathymetry and sediment layer data, respectively. Unlike the PSM approach, the PE model can incorporate range dependent bathymetry and sediment data to calculate sound pressure level in a two-dimensional $(2D)$, depth-range grid along a transect (bearing) emanating from the pile location. Thus, the PE model is implemented as an $N \times 2D$ propagation model that can quickly compute the $2D$ distribution of the pressure field along N transects surrounding a pile. Furthermore, it is suitable for low frequency calculations, (below approximately 3000 Hz) where most pile driving energy is concentrated.[11]

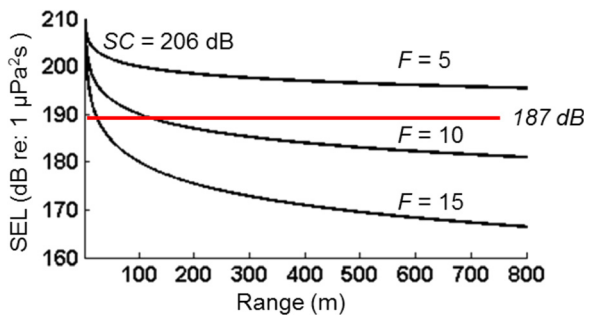

FIG. 1. (Color online) PSM solutions for F parameters of 5, 10, and 15 and a SC of 206 dB. The horizontal line corresponds to a 187 dB threshold.

For the work presented in this paper, PE calculations were carried out using the range-dependent acoustic model (RAM), a standard PE code developed by Collins.[12] RAM computes the two-dimensional, single-frequency, and range dependent Green's function,[10] $G(r, z, f)$ in the water and sediment resulting from a unit amplitude point source. Since a full spectrum and time domain analysis were desired, broadband solutions were calculated to synthesize a time domain solution.

The broadband parameters were chosen to minimize computation time while still resulting in a convergent and suitably accurate model of the pile driving noise. The frequency resolution was chosen such that the time domain period was sufficiently large to accommodate sound propagation to the extent of the simulation range.[21] Since compressional waves travel faster in the sediment than in the water, this period is determined by considering only the waveguide group velocity of the Pekeris waveguide formed by the water and top sediment layer,

$$v_g = c_w \sqrt{1 - \left(\frac{\omega_0}{\omega}\right)^2}, \tag{3}$$

where ω is the maximum simulation angular frequency and ω_0 is the waveguide cutoff frequency. The approximate cutoff frequency is

$$\omega_0 = 2\pi \frac{c_w}{2D}, \tag{4}$$

where c_w is the speed of sound in water and D is the average depth of the water column. The necessary frequency resolution is then

$$\Delta f = \frac{v_g}{R_{\max} + v_g \Delta t_s}, \tag{5}$$

where $R_{\max}$ is the maximum range of the simulation and Δt_s is the time extent of the pile source. For a maximum observation range of 800 m, the frequency step was approximately 1.5 Hz.

The minimum simulated frequency was set by the requirement of a convergent PE simulation, which was 40 Hz for this work.[21] Conversely, the maximum frequency was chosen to capture most of the signal energy, while minimizing bandwidth, and therefore computation time. The value was chosen by spectral analysis of a pile driving waveform, observed at close range. More specifically, by comparison of the summed observed energy spectral density (ESD) to the summed ESD after truncation to a variable maximum

frequency. The minimum frequency and 0.015 factor Tukey window were also applied to the truncated signal. The fraction of the total energy in the truncated simulation is given by the summed ESD ratio,

$$B = \frac{\sum ESD_{Truncated}}{\sum ESD_{Obs}}, \quad (6)$$

where ESD_{Obs} is the ESD summed over all bins in the observed measurement, $ESD_{Truncated}$ is the low-pass truncated ESD, and B is the ratio between the two. $B = 0.97$ was chosen to balance computational efficiency with accuracy. This method resulted in maximum frequencies of 2600 Hz for 24 in. (0.61 m) diameter steel piles, and 2100 Hz for 48 in. (1.22 m) diameter steel piles.

To avoid time-domain artifacts caused by interpolation, uniform depth and range steps were used for all RAM simulations. The values were obtained by application of convergence tests on the minimum, middle, and maximum simulation frequencies, and also visual inspection of each frequency component.[21] For this work, a depth step of 0.125 m and a range step of 0.5 m were used.

C. Geoacoustic model

A geoacoustic model was formulated for the region of the Columbia River between Portland, OR and Vancouver, WA in the vicinity of the new I-5 span, shown in in Fig. 2. The bathymetry was taken by fathometer measurements,[13] and describes a shallow main channel between 6 and 17 m depth. Transects were taken directly from the bathymetry and used in the propagation model.

Geophysical parameters were based upon boring studies[14] and laboratory analysis of coring samples[15] taken at several locations in the vicinity of the bridge construction. The boring records indicate three main sediment layers, shown in Table I. The medium grained sand layer contains very little non-sand content (less than 3%), and the Troutdale Formation is dense cobblestone bedrock and can be considered the acoustic basement. The large variation in the thickness of the medium sand layer occurs between the north and south riversides, with a thin layer on the north riverside that becomes progressively thicker approaching the south riverside. This variation changes the placement of the

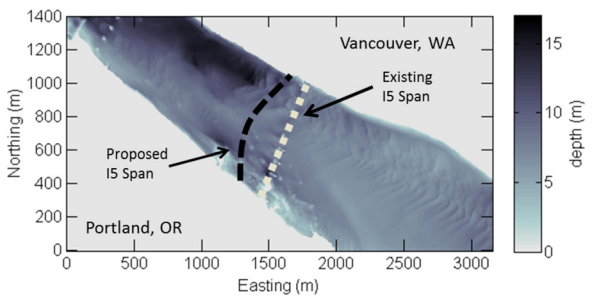

FIG. 2. (Color online) Columbia River bathymetry between Portland, OR and Vancouver, WA in the vicinity of proposed I-5 bridge construction. The gray scale corresponds to river depth and the spatial resolution in northing and easting is 2 m.

TABLE I. Geoacoustic parameters for the sediment layers.

	Density (g/cc)	Attenuation (dB/λ)	Approximate sound speed (m/s)
Water	1.00	0.00	1442
Medium grained sand	1.84	0.88	1500–1550 (Interpolated)
Medium gravel	2.15	0.88–0.75	1550–2856 (Interpolated)
Troutdale Formation	2.50	0.75	2856

highly reflective Troutdale Formation, affecting sound levels.

Three geophysical parameters were used to model each sediment layer: density, sound speed, and attenuation. For each pile, identical parameters were used although the sediment layer depths varied depending upon the location.[21]

Sediment sound speed profiles were extrapolated from geophysical boring measurements,[14] shown in Table I. Sediment density was determined from the bulk density of the coring samples and laboratory analysis that measured porosity,[16]

$$\rho_s = \epsilon\rho_w + (1-\epsilon)\rho_{sb}, \quad (7)$$

where ϵ is the sediment porosity, ρ_s is the sediment density, ρ_w is the water density, and ρ_{sb} is the sediment bulk density. Sediment attenuation is based on the viscoelastic model of Hamilton.[16] This model describes sediment attenuation that varies linearly with frequency,

$$\alpha = k_p f, \quad (8)$$

where α is the attenuation in dB per wavelength (λ) and k_p is the loss parameter. The specific loss parameters were taken from a table in the APL-UW High Frequency Ocean Environment Acoustic Models Handbook,[17] where values were chosen based on sediment description, water-sediment sound speed ratio, and sediment density. While this work corresponds to low frequency modeling, the agreement with observed measurements using these parameters implies that the linearity of sediment sound attenuation suggested by Hamilton[16] may be extended into the low frequency realm for the sediments of this study.

III. PILE DRIVING SOURCE MODEL

The pile source is accounted for with an empirical source model adapted from the Mach wave source description of Reinhall and Dahl.[8] It is an empirical model due to its dependence on a close range measured pressure field to produce agreement in spectral, time extent, and total energy characteristics. The empirical method was chosen due to the availability of close range observations. In the absence of close range measurements, modeling such as that by Zampolli[18] may be convolved with the PE simulations.

The impact between the hammer and pile is modeled as a phased point array that is tuned using measured acoustic data in the water column. To arrive at input parameters for the phased array it is assumed that a compressional wave is traveling as a bulge through the pile. The bulge travels down

the length of the pile and is attenuated upon reflection at the pile-sediment interface before traveling back up the pile. Similar to Reinhall and Dahl, it is assumed that the bulge is not attenuated as it travels along the length of the pile or as it reflects from the end of the pile that is in air above the water column.[8] The speed of the bulge propagating in the steel pile is approximately[21] $c_p = 5100\,\mathrm{m/s}$. Since this is much greater than that in the environment $(c_w = 1447\,\mathrm{m/s})$, energy is radiated in conical arrivals of incidence angle,

$$\psi = \arcsin\left(\frac{c_w}{c_p}\right), \tag{9}$$

where c_p is the speed of the deformation traveling in the pile and c_w is the speed of sound in the water.[8] Also, c_s, the sound speed in sediment, is substituted in Eq. (9) for c_w when the bulge is in the sediment rather than the water column. Each time the bulge traverses the pile, a conical arrival is generated, referred to as the mth arrival.

Figure 3 illustrates the source implementation and the first four arrivals radiating from the moving bulge at angles that are dependent on the respective sediment layer, water sound speeds, and refraction. Each mth conical arrival is formed by an array of point source solutions. This can be formulated using Huygens' principle. In cylindrical coordinates, with r measuring the distance from the pile and z measuring the depth from the surface, the expression for pressure due to the jth depth point source of the mth arrival is

$$s_{m,j}(r, z, f) = G(r, z, f)A(f)e^{-i2\pi f\tau_{m,j}}. \tag{10}$$

Equation (10) is the convolution of the broadband Green's function, $G(r, z, f)$ (point source response computed by RAM), and the empirical source model. The amplitude and phase of the source spectrum are given by the spectral weighting function, $A(f)$, and the exponential term, which contains a time delay, $\tau_{m,j}$, that depends on both the arrival number and the source depth. Note, the phase term steers the arrival to the proper incidence angle from Eq. (9) by the shift theorem.[19] The time delay is the time required for the bulge to reach the jth point source on the pile for the mth arrival, and depends on the length of the pile.

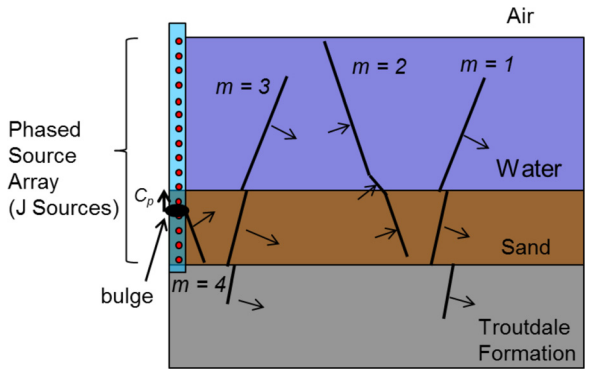

FIG. 3. (Color online) Illustration of source model implementation and the first four arrivals ($m = 1$ through $m = 4$).

Summing over all source depths results in the conical wave of the mth arrival,

$$S_m(r, z, f) = \frac{1}{J}\sum_{j=1}^{J} s_{m,j}(r, z, f), \tag{11}$$

where J is the number of point sources.

The full simulation is computed by summing over all M arrivals,

$$S_{emp}(r, z, f) = C\sum_{m=1}^{M}(-1)^{m+1}K_m S_m(r, z, f). \tag{12}$$

Here the offset C matches the energy of the simulation to that of the observation, K_m models the attenuation of the bulge at each reflection, and the $(-1)^{m+1}$ term accounts for the 180° phase shift of the bulge at reflection with the ends of the pile.

The empirical parameters, $A(f)$, C, and K_m, were derived from a close range acoustic observation of a pile driving waveform. For the derivation of the spectral weight function and attenuation constant, it was necessary to isolate the arrivals from the empirical waveform. Arrivals were isolated by determining the time separating arrivals, which depends on the motion of the bulge through the pile. The length of time from arrival m to arrival $m + 1$ is,

$$\Delta T_{m\to m+1} = \begin{cases} \dfrac{2(p_{wl-z_0})}{c_p}, & \text{if } m \text{ is odd} \\ \dfrac{2[(p_l - p_{wl}) + z_0]}{c_p}, & \text{if } m \text{ is even,} \end{cases} \tag{13}$$

where z_0 is the receiver depth, p_l is the total pile length, and p_{wl} is the wetted pile length. Odd numbered arrivals correspond to a downward traveling bulge, and even arrivals correspond to an upward traveling bulge.

The spectral weight function $A(f)$ was obtained by first isolating the first arrival using Eq. (13). The first arrival was then converted to the frequency domain using the DFT, normalized, and truncated to the bandwidth of the numerical simulation. Finally, a 0.015 factor Tukey window[19] was applied to reduce ringing in the time domain synthesis.

The attenuation factor K_m depends on the arrival number, m,

$$K_m = \begin{cases} \kappa^{(m-1)/2}, & \text{if } m = 1, 3, 5, \ldots, \\ \kappa^{m/2}, & \text{if } m = 2, 4, 6, \ldots, \end{cases} \tag{14}$$

where κ is an attenuation constant that accounts for the amplitude reduction at the bottom of the pile, and is computed empirically from the arrival amplitudes,[21] which are isolated from one another using Eq. (13). There is assumed to be no attenuation as the bulge reflects from the top of the pile or as it travels along the pile. Thus, $K_1 = 1$ (no attenuation) and then $K_2 = K_3 = \kappa$, followed by $K_4 = K_5 = \kappa^2$, etc.

The offset C was chosen such that the sum of the ESD of the simulated spectrum matches the sum of the ESD of the observed spectrum, at the observation point, over the

simulation bandwidth.[21] It is a function of the observed and simulated signals,

$$C = \frac{\sum ESD_{Observed}}{\sum ESD_{Simulated}}. \quad (15)$$

The broadband Green's function solutions of Eq. (12) represents the complex pressure at each point in the simulation area. The source model is visualized using a short-range synthesis of this frequency domain solution, which is converted to sound pressure level (SPL) and shown in Fig. 4 at times of 5, 10, 20, and 30 ms. From the impulse bulge, conical waves radiate uniformly into the water and sediment at the angles predicted by Eq. (9).

IV. RESULTS

Acoustic measurements were taken by the consulting firm David Evans and Associates[20] in February 2011 for test pile operations in the Columbia River as shown in Fig. 5. On both the north (pile site B) and south (pile site A) riversides, piles with diameters of 24 and 48 in. (0.61 and 1.22 m) were driven into the sediment in the areas indicated by white rectangles in Fig. 5. On the north riverside, the 24 and 48 in. piles were labeled B1 and B2, respectively. Similarly, on the south riverside, the 24 and 48 in. piles were labeled A1 and A3, respectively.

For each pile site (A and B) the impact waveforms were recorded at five measurement ranges, which were aligned in a direction parallel to the river bank. A single hydrophone was located in the middle of the water column at each measurement location. At each pile driving site, the closest measurement position was 10 meters from the pile, and three remote monitoring stations were positioned (downstream from site A and upstream from site B) at distances of 200, 400, and 800 m from the pile sites. The acoustic data at these four locations were recorded by a Cetacean Research

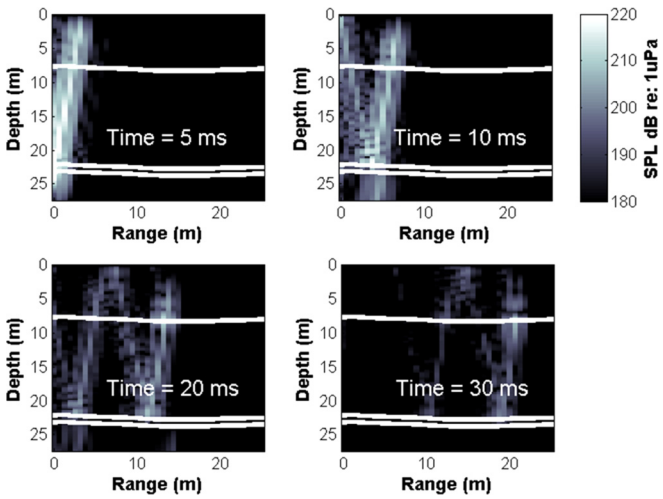

FIG. 4. (Color online) Short-range snapshot of SPL for the empirical source model. The gray scale corresponds to SPL and the white horizontal lines demarcate the sediment layer boundaries. The top layer is the water column, followed by sand, gravel, and the Troutdale Formation, descending downward. Four arrivals were used for the empirical source model.

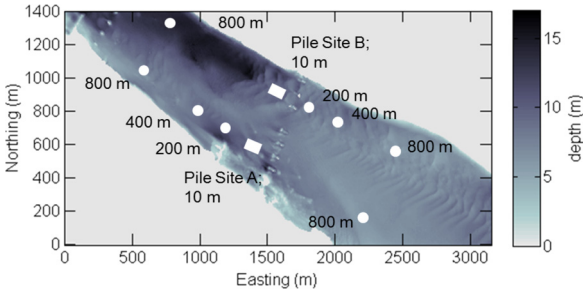

FIG. 5. (Color online) Monitoring locations of test pile operations in the Columbia River. Locations along the north and south riversides correspond to pile sites B and A, respectively.

Technology (CRT) model CR1 hydrophone with −198 dB (re: 1 V/Pa) transducer sensitivity.[20] An additional remote measurement point was positioned 800 m from the pile site in the opposite direction (i.e., upstream from site A and downstream from site B) where measurements were recorded with a CRT CR55 hydrophone with −165 dB (re: 1 V/Pa) sensitivity.[20] Thus, the five observation points at each of four pile driving locations provided a total of 20 measurements for this study. In Fig. 5, the remote measurement points are indicated by white circles, and the closest measurement locations are not shown.

Simulations were computed along the paths of the acoustic observations and accounted for the corresponding bathymetry, geological configurations, and test pile dimensions. In each case, the closest measurement location (10 m from the pile driving site) were used to compute the empirical parameters, $A(f)$, C, and K_m as described in Sec. III. The geoacoustic parameters from Table I were used with parameters specific to each test pile, as summarized in Table II. These parameters include the pile dimensions, sediment depths, and the empirically derived parameters. The number of sources in Eq. (11) was $J = 100$ for each frequency, which were uniformly distributed along the length of the pile listed in Table II.

In Table II it is observed that the larger piles produce both higher sound levels, reflected by the higher offset, C, and greater energy concentration in the lower frequencies, shown by the lower maximum frequency. The normalized spectral weight functions, $A(f)$, derived from the 10 m observations taken near each pile are shown in Fig. 6. Most of the energy is concentrated below 2600 Hz for the smaller

TABLE II. Modeling parameters for each of the four piles.

Pile ID	B1	B2	A1	A3
Diameter (m)	0.61	1.22	0.61	1.22
Length (m)	27.75	29.25	24.75	40
Wetted length (m)	22.5	23.5	18.25	33.5
Gravel depth (m)	14.5	14.5	60	60
Bedrock depth (m)	15.5	15.5	62	62
Offset C (dB)	90.2	96.7	91.1	100.0
Attenuation constant κ	1/3	1/5	2/5	2/5
Maximum frequency (Hz)	2600	2050	2600	2100

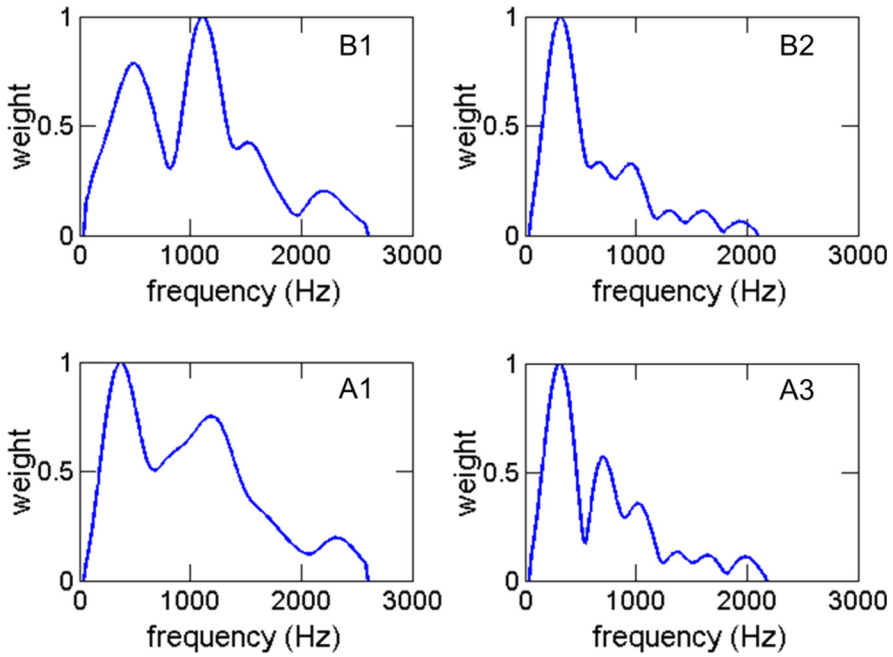

FIG. 6. (Color online) The normalized spectral weight functions, $A(f)$, for piles B1, B2, A1, and A3. Most of the energy is concentrated below 2600 Hz for the smaller diameter piles (B1 and A1) and below 2100 Hz for the larger diameter piles (B2 and A3).

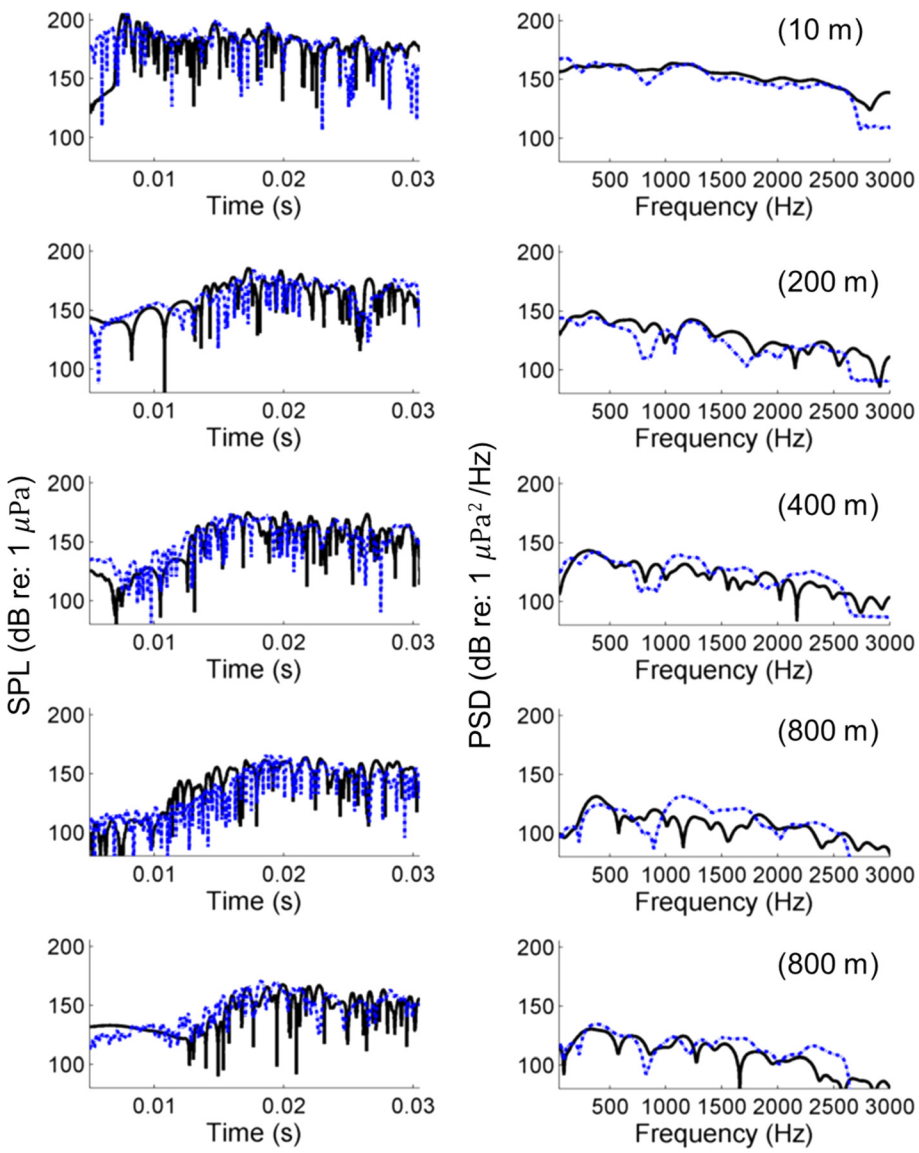

FIG. 7. (Color online) SPL (left) and PSD (right) comparisons for pile B1 at distances of 10, 200, 400, and 800 m. At each range position, the phone depth was half the water column depth (Ref. 20). The solid line corresponds to the observations and the dashed line corresponds to simulated results. The second 800 m observation is the single observation at the opposite bearing angle. (See Fig. 5.)

diameter piles (B1 and A1) and below 2100 Hz for the larger diameter piles (B2 and A3).

SPL and power spectral density (PSD) are compared to each observation of pile B1 in Fig. 7, which is consistent with similar comparisons for the other piles.[21] SPL comparisons show good agreement in the absolute levels over time at all location. Matching specific peaks and nulls was intractable beyond the 10 m observation due to a number of factors including uncertainties in the measurement locations as well as the material parameters, water depths, and sediment depths. PSD comparisons show good agreement in both levels and roll off at all ranges, with excellent agreement below 500 Hz. Beyond the close range comparisons, the continued agreement in roll off indicates that the geoacoustic model is attenuating the noise accurately over the entire frequency band.

In Fig. 8 the SEL predicted by the model is compared with the measured values at each location for each of the four pile sites. The x marks represent simulated data, the o marks represent observed data, and the dotted lines correspond to results using the PSM. The top dotted line corresponds to an F factor of 5 and the bottom an F of 20, and the middle dotted line is a fit to the data, and corresponds to an F of 10.5. In each case depth of the measured and modeled SEL is the middle of the water column.[21] For 19 of the 20 comparisons, the model agrees with the observations to within 3 dB. At the closer observation locations, the agreement was within 3 dB at all four pile driving locations, which suggests highly reliable predictions within 400 m. The single large disagreement of about 8 dB occurred at pile site B, where there is more uncertainty in the sediment parameters/thickness due to the shallower bedrock layer. Even with these discrepancies, the computational model improves upon the fit curve produced by the PSM. Note that the fit curve ($F = 10.5$) is based on the acoustic observations,[21] which this method has improved upon with only a single acoustic measurement.

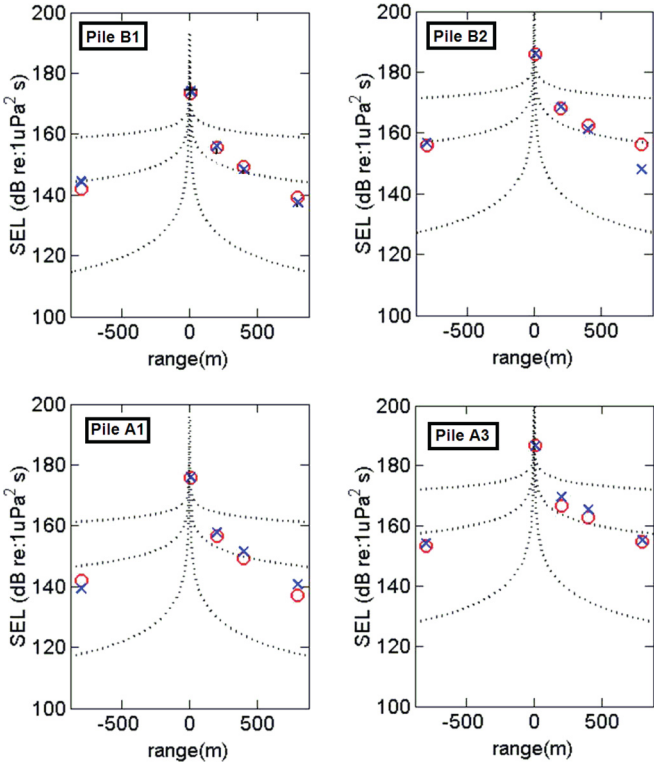

FIG. 8. (Color online) Sound exposure level summaries for each pile. The × marks represent simulated data, the ○ marks represent observed data, and the dotted lines correspond to results using the PSM. The top dotted line corresponds to an F factor of 5 and the bottom an F of 20, and the middle dotted line is a fit to the data, and corresponds to an F of 10.5. In each case depth of the measured and modeled SEL is the middle of the water column.

V. APPLICATIONS

In Sec. IV the validity of the computational method was established by comparing simulation results with acoustic observations. Subsequently the model was applied to predict SEL over large portions of the Columbia River and characterize the effects of variable bathymetry as well as various hypothetical sediment configurations.

Figure 9 shows SEL predictions about pile B1. While the PSM predicts concentric circles surrounding the pile, inhomogeneities in sediment and bathymetry produce significant variations from this simplified prediction. One interesting transect is to the northwest of the pile. While deeper water causes less attenuation over long range (discussed below), this area results in very sudden attenuation. This particular discrepancy is caused by greater spreading in the region beyond the sudden increase in bathymetry depth along the transect. None of these significant variations would be predicted by the PSM, which highlights the value of more advanced modeling.

The hybrid PE/empirical source modeling approach was also applied to quantify the effects of variable bathymetry and various alternate (hypothetical) sediment configurations. Three parameter studies are carried out to test the effects of changing (A) the bathymetry profile, (B) the geoacoustic properties of the top sediment layer, and (C) the depth of the highly reflective bedrock layer (Troutdale Formation). These range dependent variation analyses were performed by computing otherwise equivalent simulations and varying only the parameter of interest. The effects of bathymetry were analyzed by selecting extreme test cases from the local

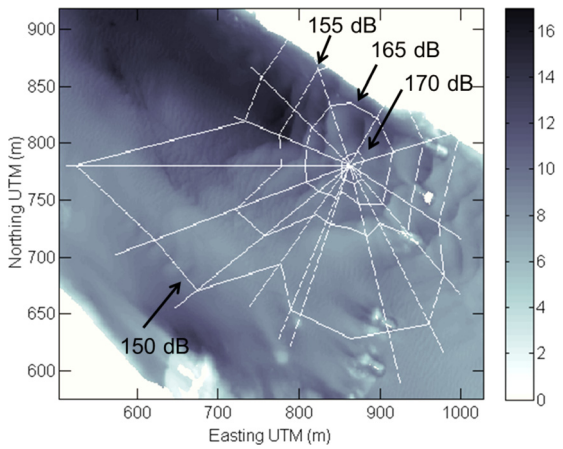

FIG. 9. (Color online) SEL contour plot about pile B1. The radial lines demarcate two-dimensional simulation results, and the lines connecting radials connect points of equivalent SEL.

Columbia River bathymetry, shown in Fig. 10. Analysis of the effect of the top sediment layer was done by comparing simulated results using published parameters[17] that describe the alternative sediments listed in Table III. Sediments with partial sand compositions were selected for this analysis to examine the effects of mixing additional soil components into the sandy bottom of the Columbia River. Finally, the effect of the depth of the Troutdale formation was studied by computing solutions with the top interface of the Troutdale formation located at various depths in the simulation space. The results of the three analyses described above are shown in panels (A), (B), and (C) of Fig. 11.

Panel (A) of Fig. 11 indicates that for most of the variable bathymetry test cases there are only local variations of less than 5 dB, and only the average water depth over long distances significantly affects sound levels. At distant ranges, the greatest attenuation is observed in the shallow flat case due to increased sediment interactions over long range. Examining the SEL curve corresponding to the rough bathymetry, deeper sections produce lower sound levels as the sound freely expands into a greater area, but sound levels increase in the shallower regions as the signal energy is concentrated into the smaller area.

Panel (B) of Fig. 11 shows the results of comparing the various hypothetical top layer sediments listed in Table III. There is a large complex SEL dependence on density, sound speed, and attenuation, with no single geoacoustic parameter having a dominant effect. The SEL curves are similarly shaped for each hypothetical sediment top layer scenario except sandy clay, where there is a dramatic spike at 370 m.

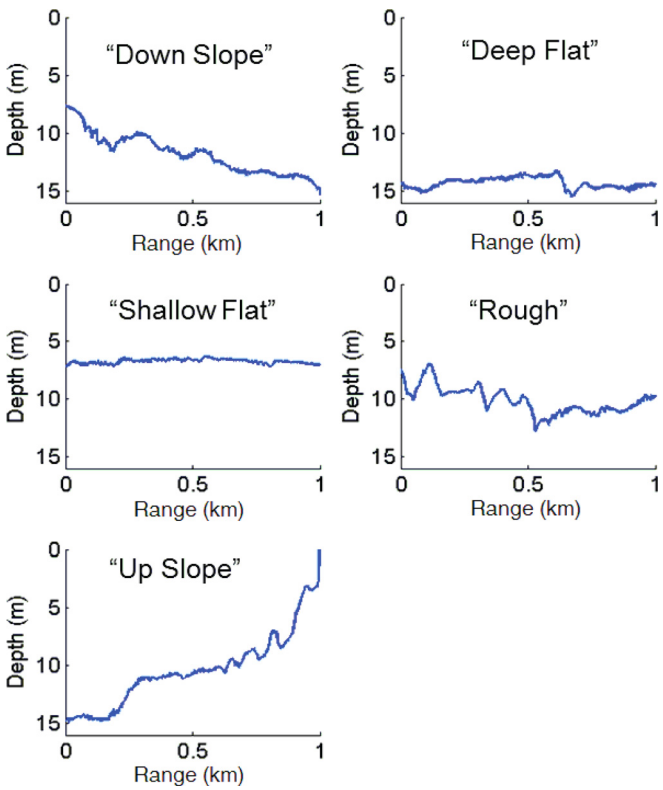

FIG. 10. (Color online) Bathymetry slices from the Columbia River between Portland, OR and Vancouver, WA. Slices were chosen to encompass the extremes of the local area.

TABLE III. Geoacoustic parameters of various hypothetical alternatives to the top sediment layer.

	Density (g/cm^3)	Attenuation (dB/λ)	Sound speed (m/s)
Sandy clay	1.147	0.089	1420
Sandy mud	1.490	0.211	1420
Sandy gravel	2.492	0.931	1936
Coarse silt	1.195	1.177	1472

In this case, the impact waveform is attenuated very little in the sediment, and the large spike corresponds to the reflection of the first arrival from the Troutdale formation.

Panel (C) of Fig. 11 indicates that the effect of the bedrock depth alters sound levels consistently over range, with the shallowest bedrock layer scenario having the greatest effect. Bedrock layers with depths greater than 25 m have little practical effect on the simulated SEL in the water column for the medium sand top layer of the Columbia River.

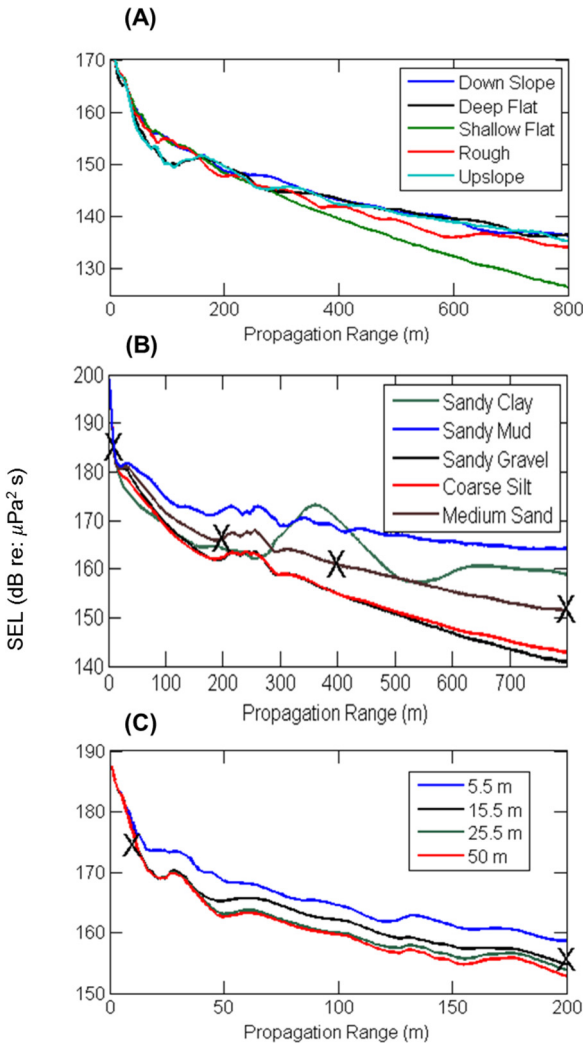

FIG. 11. (Color online) Range dependent SEL at a depth of 3.5 m for various bathymetry profiles and hypothetical sediment configurations. Panel (A) corresponds to the bathymetry test cases shown in Fig. 10, panel (B) corresponds to the hypothetical top sediment layer parameters listed in Table III, and panel (C) corresponds to the variable bedrock depths shown in the legend. The × marks denote the acoustic observations.

VI. CONCLUSION

This paper presented a computational method to both analyze and predict the underwater noise produced by pile driving. The hybrid method utilizes an empirical model of the pile driving source, coupled to a broadband synthesis of PE propagation. Simulations used a sediment model and bathymetry that are range dependent.

The proposed method was shown to be in good agreement to observations of test pile operations in the Columbia River between Portland, OR and Vancouver, WA. SPL levels were accurately predicted and most of the features in the observed data were predicted at close range. PSD comparisons showed levels and roll off in good agreement, and SEL agreed within 3 dB in 19 of 20 comparisons. Within the 400 m range, SEL showed very good agreement at all observation locations.

Finally, the hybrid PE/empirical source modeling approach was applied to produce SEL predictions in the Columbia River and study the effects of various bathymetry profiles and hypothetical sediment configurations. The absolute depth of the bathymetry was found to be the only factor that significantly affects long-range sound levels, while bathymetry variations create localized effects. The top sediment layer was shown to effect sound levels greatly depending on all input geoacoustic parameters. Also, the bedrock layer was determined to be insignificant when deeper than 25 m for the medium sand top layer present in this region of the Columbia River.

ACKNOWLEDGMENTS

The authors would like to thank the Oregon Department of Transportation and Federal Highway Administration for supporting this work. Furthermore, the authors would like to acknowledge David Evans and Associates, Inc. for providing the pile driving monitoring data and the Columbia River Crossing for providing the sediment geotechnical survey data. The authors acknowledge and congratulate N.L. for the completion of his Master's degree in Electrical Engineering from Portland State University. N.L. performed all of the acoustic simulations and data analysis results presented in this paper. The thesis[21] provides a thorough treatment of this research topic, as well as finite difference time domain pile driving simulations that could not be included here.

[1]J. A. Reyff, "Underwater sound pressure levels associated with marine pile driving," Transp. Res. Rec. special volume CD **11-S**, 481–490 (2005).

[2]M. C. Hastings and A. N. Popper, "Effects of sound on fish," report to Jones & Stokes Associates, Inc. for California Department of Transportation (2005), http://www.dot.ca.gov/hq/env/bio/files/Effects of Sound on Fish23Aug05.pdf (Last viewed 7/25/2014).

[3]S. Hardyniec and S. Skeen, "Pile Driving and Barotrauma Effects," Trans. Res. Rec. **1941**, 184–190 (2005).

[4]C. Mueller-Blenkle, P. K. McGregor, A. B. Gill, M. H. Andersson, J. Metcalfe, V. Bendall, P. Sigray, D. Wood, and F. Thomsen, "Effects of pile-driving noise on the behaviour of marine fish," COWRIE Ltd., Ref: Fish 06-08 / Cefas Ref: C3371 Technical (2005).

[5]J. A. David, "Likely sensitivity of bottlenose dolphins to pile-driving noise," Water Env. J. **20**, 48–54 (2006).

[6]J. Carstensen, O. D. Henriksen, and J. Teilmann, "Impacts of offshore wind farm construction on harbour porpoises: Acoustic monitoring of echolocation activity using porpoise detectors (T-PODs)," Mar. Ecol. Prog. Ser. **321**, 295–308 (2006).

[7]ICF Jones & Stokes Associates, Inc. and Illingworth and Rodkin, Inc., "Technical guidance for assessment and mitigation of the hydroacoustic effects of pile driving on fish," California Department of Transportation report, 2009.

[8]P. G. Reinhall and P. H. Dahl, "Underwater Mach wave radiation from impact pile driving: Theory and observation," J. Acoust. Soc. Am. **130**(3), 1209–1216 (2011).

[9]C. Erbe, "Underwater noise from pile driving in Moreton Bay, QLD," Acoust. Austr. **37**, 87–92 (2009).

[10]F. B. Jensen, W. A. Kuperman, M. B. Porter, and H. Schnidt, *Computational Ocean Acoustics* (AIP, Woodbury, NY, 1994), pp. 118–133, 457–527.

[11]M. L. Stockham, P. G. Reinhall, and P. H. Dahl, "Characterizing underwater noise from industrial pile driving at close range," in *Proceedings of IEEE Oceans* (IEEE, 2010).

[12]M. D. Collins, "A split-step Padé solution for the parabolic equation method," J. Acoust. Soc. Am. **93**, 1736–1742 (1993).

[13]David Evans and Associates, Marine Services Division, http://deamarine.com (Last viewed 7/25/2014).

[14]CRC Geotech Reports, Appendix A: Boring Logs, Columbia River Crossing (2009).

[15]CRC Geotech Reports, Appendix F: Laboratory, Columbia River Crossing (2009).

[16]E. L. Hamilton, "Columbia River Crossing test pile project hydroacoustic monitoring final report," Columbia River Crossing (1980).

[17]Applied Physics Laboratory (APL), "APL-UW high-frequency ocean environmental acoustic models handbook," TR9407, APL, University of Washington, October (1994), http://staff.washington.edu/dushaw/pubs.html (Last viewed 7/25/2014).

[18]M. Zampolli, M. J. J. Nijhof, Christ A. F. de Jong, M. A. Ainslie, E. H. W. Jansen, and B. A. J. Quesson, "Validation of finite element computations for the quantitative prediction of underwater noise from impact pile driving," J. Acoust. Soc. Am. **133**(1), 72–81 (2013).

[19]E. C. Ifeachor and B. W. Jervis, *Digital Signal Processing: A Practical Approach* (Addison-Wesley, New York, 1993), pp. 104–134, 697–700.

[20]David Evans and Associates, "Columbia River Crossing test pile project hydroacoustic monitoring final report," Columbia River Crossing (2011).

[21]N. D. Laws, "A parabolic equation analysis of the underwater noise radiated by impact pile driving," Master's thesis, Portland State University, March (2013).